Predicting Two-Dimensional Silicon Carbide Monolayers

Zhiming Shi[†,‡], Zhuhua Zhang[‡], Alex Kutana[‡] and Boris I. Yakobson[*‡]

[†]Institute of Theoretical Chemistry, Jilin University, Changchun 130023, People's Republic of China

[‡]Department of Materials Science and NanoEngineering, Department of Chemistry, and the Smalley Institute for Nanoscale Science and Technology, Rice University, Houston, Texas 77005, United States.

[*]Address correspondence to: biy@rice.edu

ABSTRACT:

Intrinsic semimetallicity of graphene and silicene largely limits their applications in functional devices. Mixing carbon and silicon atoms to form two-dimensional (2D) silicon carbide (Si_xC_{1-x}) sheets is promising to overcome this issue. Using first-principles calculations combined with the cluster expansion method, we perform a comprehensive study on the thermodynamic stability and electronic properties of 2D Si_xC_{1-x} monolayers with $0 \leq x \leq 1$. Upon varying the silicon concentration, the 2D Si_xC_{1-x} present two distinct structural phases, a homogenous phase with well dispersed Si (or C) atoms and an in-plane hybrid phase rich in SiC domains. While the in-plane hybrid structure shows uniform semiconducting properties with widely tunable band gap from 0 to 2.87 eV due to quantum confinement effect imposed by the SiC domains, the homogenous structures can be semiconducting or remain semi-metallic depending on a superlattice vector which dictates whether the sublattice symmetry is topologically broken or not. Moreover, we reveal a universal rule for describing the electronic properties of the homogenous Si_xC_{1-x} structures. These findings suggest that the 2D Si_xC_{1-x} monolayers may present a new "flatland" of 2D materials, with a rich variety of properties for applications in electronics and optoelectronics.

KEYWORDS: two-dimensional alloy • silicon carbide •semiconductor • first-principle calculation • cluster expansion

Since the discovery of graphene in 2004,[1] two-dimensional (2D) atomic crystals have stimulated extensive research activities due to a number of unusual properties and potential applications in next-generation devices.[1-3] Silicon, on the other hand, is the backbone material of the current semiconductor industry, and will continue to play a key role in future nanotechnology. Silicene, the silicon analogue of graphene, has recently become a new popular 2D material not only due to its Dirac electronic dispersion at the Fermi level (similar to graphene)[4-7] but also because of its compatibility with current Si-based electronics. A number of experiments have realized the epitaxial growth of silicene on some metal substrates, such as Ag,[8-11] Ir,[12] and ZrB_2.[13] However, both graphene and silicene exhibit zero band gaps, making them unsuitable for electronic devices with logic operation. To overcome this issue, extensive research efforts have been devoted to realize a controllable band gap in these materials. Several strategies, such as patterning into nanoribbons,[14] applying an electrostatic gate[15] and using chemical functionalization,[16] have been proposed to effectively open a band gap in graphene and silicene. Although these strategies are useful for certain applications, realizing a band gap in the range of 1.0−2.0 eV, which is required for room temperature operation, remains a challenging task, in particular when electron mobility needs to be less compromised.

Beyond graphene and silicene, the research enthusiasm on 2D materials has been largely extended into other inorganic 2D materials. In recent years, there have been numerous 2D materials reported, such as BN,[17-18] SiC,[16, 19] CN,[20] ZnO[21] and MS_2[17, 22] *etc*. However, the quest of semiconducting 2D materials is among the most research attention. Especially, it is desirable to realize a 2D semiconductor with strong in-plane covalent bonds that can resist large mechanical deformation and external chemical corrosion. In this respect, the 2D silicon carbide monolayer represents an ideal candidate as not only does it shows a 2.52 eV band gap[16] but also inherits the robust structure from graphene. Very recently, Lu *et al*. predicted a new Si-C monolayer, known as g-SiC_2,[23] which has a desirable band gap of 1.1 eV and holds great promise for optoelectronic applications. An overview of theoretical progress in this field suggests that changing the stoichiometry and bonding structure of the 2D Si-C monolayers can lead to remarkably different properties, as demonstrated in the pt-SiC_2,[24] and SiC_3.[25] Recently, Gao performed a comprehensive structure search based on particle-swarm optimization method, and found that graphite-like Si−C structures are strongly favored, even though a cubic SiC_3 structure is exceptionally stable at this specific composition.[26] However, the study of 2D Si-C system is still limited to several scattered results, and a full physical picture describing their structures and functions as well as the electronic tunability remains far from obvious. Compared with the commonly used strategies, alloying carbon and silicon atoms in such two dimensional binary systems will be particularly interesting, as it

promises composition-modulated electronic structures. To this end, several fundamental issues must be addressed: (i) what are their favorable structures at different C:Si ratios? (ii) Are all the structures semiconducting? (iii) what is the relationship between their structures and functions?

In this work, based on first-principles calculations combined with cluster expansion (CE) approach, we perform a comprehensive study to explore the structural and electronic properties of the monolayer Si_xC_{1-x} materials. The CE method has been successfully used before to explore the alloyed and adsorbed 2D systems.[27-30] The 2D Si_xC_{1-x} presents two distinct structural phases, homogenous phase and in-plane hybrid phase with SiC domains. The in-plane hybrid phase shows uniform semiconducting properties with widely tunable band gaps due to quantum confinement effect imposed by the SiC domains. In contrast, the homogenous structures can be either semiconducting or semi-metallic depending on a superlattice vector, which complies with a universal rule similar to the gap-chirality relationship in carbon nanotubes. Our findings open a new way to designing 2D semiconductive atomic crystals alloyed by earth-rich silicon and carbon and might guide the fabrication of functional devices compatible with current silicon electronics.

RESULTS AND DISCUSSION:

We obtain values of 1.42, 2.27and 1.79Å for the C-C, Si-Si and C-Si bonds in pristine graphene, silicene and SiC monolayers, respectively, and the buckling height of the silicene is 0.45 Å, in agreement with previous results.[7, 31] The Si_xC_{1-x} sheet can be viewed as graphene (or silicene) with substitutional doping of Si (or C) atoms in different concentrations. As has been established, graphene is a pure planar monolayer, while silicene undergoes a slight out-of-plane buckling, due to the preference of sp^3 hybridization for Si atom. We perform test calculations to examine whether we should consider buckling in Si_xC_{1-x} sheet. We first choose the planar $Si_{0.5}C_{0.5}$, which is composed of only Si-C bonds, and purposely introduce buckling along the normal direction; the buckling simply disappears after relaxation by first-principle calculation, implying that the Si-C bonds prefer sp^2 hybridization rather than sp^3 hybridization. Therefore, we introduce buckling only for the second half CE-2 ($x_{CE\text{-}2}$=0.5~1with Si-Si bonds), while for CE-1 ($x_{CE\text{-}1}$=0~0.5 without Si-Si bonds) all the structures are set planar (see insets of Figure 1e). Over 300 structures are predicted and tested by DFT calculation when varying x from 0 to 1. We are aware that in our structural search the Si (or C) atoms are restricted to the same honeycomb sublattices. However, our testing calculations confirm that the structures allowing Si atoms to distribute on different sublattices correspond to high-energy states. This is also consistent with the prediction by Ding and coworkers that the Si dopants in the 2D SiC_3 sheet preferably sit at the same sublattice rather than at the different sublattices.[25]

Among the obtained >300 structures in the CE-1 and CE-2 calculations, we mainly focus on the 30 structures with the lowest formation energy at each concentration, with 15 structures in each half. We optimize the 30 structures with refined parameters to get more precise atomic structure and total energy, and their atomic configurations are displayed in Figure S1 and S2. Interestingly, these structures can be classified into two phases: the in-plane hybrid phase rich in SiC domains (Figure 1a and d) and the homogenous phase (Figure 1b and c). For convenience, we refer to the minority element as dopant. For the in-plane hybrid phase, SiC domains separate the graphene (or silicene) sheet into nanoribbons, while for the latter phase the Si (or C) dopants are uniformly dispersed in the graphene (or silicene) sheet. The stability of these structures can first be evaluated by comparing their E_{coh} and δF, as summarized in Figure 1e and f. The straight line connects E_{coh} and δF of graphene and silicene at x=0 and 1, respectively. Negative values of E_{coh} indicate that all the 30 structures are energetically favorable, and their relative stability can be easily measured by comparing the altitude δF from the line. The SiC monolayer (*i.e.* x=0.5) is shown to be thermodynamically stable since its δF is below the straight line with a negative δF of −0.016eV, whereas all the remaining Si_xC_{1-x} structures have their δF located above this line and thus are metastable with respect to graphene and silicene. However, δF for these structures are distributed within a very narrow range of 0.057-0.329 eV, suggesting their considerable stability. It is also worthwhile to mention that the ground states at x=0.25 and x=0.33 are pretty the same structures as the recently reported 2D SiC_3[25] and g-SiC_2[23] sheets obtained by the particle-swarm optimization method. More interestingly, at x=0.2 and x=0.4, our CE-predicted ground states are more stable by 11 and 50 meV/atom than the SiC_4 and Si_2C_3[32] obtained using the particle-swarm optimization technique. The computed phonon spectra of the new SiC_4 and Si_2C_3 are plotted in Figure S3. Clearly, the absence of imaginary frequencies indicates the inherent dynamical stability. To make our predictions more convincing, we further performed a global minimum search for the 2D $Si_2C_3$with fixed composition using CALYPSO package,[33] free of hexagonal mesh limitations. The same structures composed exclusively of hexagons, as predicted by the CE method, were reproduced when the generated structures amount to 900. These facts give us confidence in the CE method for reaching the ground states of 2D alloy structures. In addition to the thermodynamic stability, we also examine the dynamic stability by using ab initio MD simulations. The simulations were performed with 2×2 supercells for the structures at x=0.1(in-plane hybrid), x=0.167(spatially well dispersed) and x=0.22(largest δF value of 0.329eV) at temperature of 2500 K. No remarkable structural disruption is observed in the three structures throughout 10 ps simulations (see snapshot in Figure S4), confirming their robust structures against thermal fluctuation at high temperature.

Having established the favorable structures of 2D SiC sheets, we proceed to explore their novel properties. First, we examine the most important electronic parameter, the band gap of these 2D SiC sheets. A rich variety of electronic properties, such as indirect (black hollow hexagons), direct (red solid hexagons) gaps and semi-metallic (blue solid triangles) behaviors appear when x changes from 0 to 1, as shown in Figure 2. Most of the Si_xC_{1-x} sheets exhibit semiconducting properties, while only two homogenous structures, $Si_{0.17}C_{0.83}$ and $Si_{0.17}C_{0.83}$, are semimetallic, akin to graphene and silicene. Generally, the band gap first increases with increasing x and reaches a peak of 2.87eV at x=0.5 (2D silicon carbide), beyond which the band gap drops to 0 eV as x further increases to 1. The entire plot of band gap resembles a volcano plot characterizing the catalyst performance. It can be concluded that the band gap of Si_xC_{1-x} sheets is proportional to the Si (or C) doping concentration in graphene (or silicene). Here, we analyze the first half of x=0~0.5 to reveal the mechanism for the gap opening, and similar mechanism should hold for the other half. Generally, due to difference in electronegativity between C and Si atoms, valence electrons of Si tend to transfer to the nearest C atoms in the Si_xC_{1-x} sheets, and C-Si bonds show ionic character as shown in the background of Figure 3c. The delocalized π electrons in graphene become localized by introducing Si dopants due to the potential perturbation. As the doping concentration increases, C-Si bonds proliferate, leading to more significant localization of the π electrons, giving rise to the increase of band gaps with x. The silicon carbide (Si:C=1:1) represents the extreme, in which all the bonds are ionic maximizing electronic localization. Increasing x further, the proportion of Si-C bonds starts decreasing and, as a consequence, the band gap decreases. As the GGA underestimates the band gap of most semiconductors, we perform test calculations using the hybrid HSE06 functional and do not find qualitative changes in our conclusions. For example, the band gap of the $Si_{0.1}C_{0.9}$ is just enlarged from 0.60 eV calculated with GGA to 0.72eV obtained with HSE06. Considering the computational cost, we mainly focus on the GGA results in the following discussions.

Next, we take the $Si_{0.1}C_{0.9}$ as a model to further explore the detailed structural and electronic properties of the in-plane hybrid Si_xC_{1-x} sheets. The atomic structure of $Si_{0.1}C_{0.9}$ is shown in Figure 3a, where the shaded regions, each containing a SiC chain, stand for the SiC domains and divide the sheet into parallel aligned armchair C ribbons. The energetic preference of such an in-plane heterostructure suggests that the SiC and C tend to undergo a phase separation at this specific concentration. The corresponding band structure in Figure 3b shows a direct band gap of 0.60 eV, which forms near the middle point of the line from the Γ to M1. It is well known that quantum confinement effect is the main factor causing a non-zero band gap in graphene nanoribbons[34] as well as in graphene-BN hybrid structures.[35] If the SiC chains are considered as the BN domain or a vacuum region, similar mechanism should be anticipated for the band gap opening in the $Si_{0.1}C_{0.9}$ structures. To verify this mechanism, we

examine the difference between the deformation electrostatic potential, which is defined as the total electrostatic potential of the $Si_{0.1}C_{0.9}$ structures subtracting the sum of isolated atoms. Figure 3c presents the plane-averaged electrostatic potential different. Obviously, the potential of SiC chains rises to 0.22eV while that of armchair C ribbons is lowered by 0.04~0.10 eV. The band gap opening of the $Si_{0.1}C_{0.9}$ sheet results from the quantum confinement due to the potential well within the C ribbon. The same results can be found in $Si_{0.9}C_{0.1}$ sheets of hybrid phase (as shown in Supporting Information Figure S5). Generally, the sheet with a wider C domain has a smaller band gap, supporting the quantum confinement as a dominating mechanism for the band gap opening. However, due to the very narrow widths of the SiC and C domains, the electronic states from different domains are strongly overlapped. Therefore, the $Si_{0.1}C_{0.9}$ structure behaves more like an electronic alloy, rather than a true electronic heterostructure. This is indeed reflected in the plots of partial charge density which shows that the near-gap electronic states are distributed in both the SiC and graphene domains (as shown in Figure 3b), in particular for the charge density distribution of the valence band maximum (VBM). Enlarging the domain width may transform the system into an in-plane electronic heterostructure that can confine charge carriers inside a specific type of domains, which will be an interesting topic for future works.

In what follows, we turn to discuss the homogenous structures of the Si_xC_{1-x} sheets. Within the ground state structures, we find three homogenous structures, $Si_{0.17}C_{0.83}$, $Si_{0.33}C_{0.67}$ and $Si_{0.83}C_{0.17}$, which have the dopants atoms spatially well dispersed within the graphene (x<0.5) or silicene (x>0.5) framework. Besides, some metastable structures are also found in the homogenous phase, mostly distributed in the range $0.125<x<0.333$ and $0.667<x<0.928$. A common feature in these structures is their three-fold symmetry, like the 2D SiC sheet. We find that the homogenous sheets show richer electronic properties, which can either be semiconductive (e.g. $Si_{0.33}C_{0.67}$) or semimetallic (e.g. $Si_{0.17}C_{0.83}$ and $Si_{0.83}C_{0.17}$), in sharp contrast to the in-plane hybrid ones that show uniform semiconductive properties. To gain deeper insight into the structure-property relationship, we set up a structural description for the homogenous Si_xC_{1-x} sheets by defining a superlattice vector $\mathbf{R} = n\mathbf{a_1} + m\mathbf{a_2}$ connecting two neighboring dopants Si (or C), where $\mathbf{a_1}$ and $\mathbf{a_2}$ are the primitive lattice vectors of graphene, as illustrated in the inset of Figure 4a. With this description, $Si_{0.17}C_{0.83}$ and $Si_{0.33}C_{0.66}$ can be represented as $\mathbf{R} = 1\mathbf{a_1} + 1\mathbf{a_2}$and $\mathbf{R} = 1\mathbf{a_1} + 0\mathbf{a_2}$, which are marked as (1,1) and (1,0), respectively. To make our analysis more general, we also design several homogenous Si_xC_{1-x} sheets, whose doping concentrations are beyond what the CE calculations have shown, and their superlattice vectors are supplementary to those of the predicted structures. Figure 4a summarizes band gaps for the homogenous Si_xC_{1-x} sheets ranging from (1,0) to (3,1). Both Si doping of graphene (blue line) and C doping of silicene (red line) are considered in our computation, and detailed band structures are displayed in Figure S6 (Si dopant in graphene) and Figure

S7 (C dopant in silicene). It is found that all the structures with (n-m)mod3 = ±1 possess sizeable energy gaps ranging from 0.137 to 0.726 eV, while the rest with (n-m)mod3 = 0 remain semimetallic, complying with a similar gap-chirality relationship as in CNTs,[36] yet opposite to the previously revealed rule for antidot graphene.[37] With this rule, it is easy to deduce that all the homogenous sheets with a superlattice vector along armchair directions retain semi-metallic behavior, while those with the vector along the zigzag or random directions can be either semiconductors or semimetals depending on (n-m)mod3. This is somewhat surprising in a sense that the electronic property of Si_xC_{1-x} sheets can be independent of spatial ordering of dopants. The distinct superlattice vector-gap dependence in such pure 2D systems thus calls for an explanation.

We take the (1,0), (1,1) and (2,0) structures as examples to clarify the underlying mechanism. Firstly, the energy-resolved charge density is employed to identify the difference between the CBM and VBM as shown in Figure 4b, c and d. It is shown that the VBM of the (1,0) and (2,0) is originated from the π electrons of carbon atoms on the same sublattice, while CBM is dominated by the π^* electrons of the Si and C atoms on the other sublattice. It appears that the symmetry of sublattices in the (1,0) and (2,0) are broken by Si doping, and thus the origin of band gap is due to the staggered sublattice potentials. This is very similar to the band gap in h-BN that is due to the ionic potential difference between B and N atoms. The electrons need to overcome the barrier formed by the sublattice potential difference when transferring from VBM to CBM. The situation becomes different in the band structure of the (1,1) structure, in which we observed two graphene-derived linear bands around the Fermi level. The two linear bands are a characteristic of a semimetal, despite a tiny band gap formed slightly below the Fermi level. The charge densities corresponding to the two bands uniformly reside on all the C atoms (on different sublattices), and little on Si atoms. Therefore, the two C sublattices in the (1,1) structure remain symmetric, and the Dirac cone survives from the doping of Si atoms. In addition, we identify a double-degenerate impurity-like band (blue one in Fig. 4c) below the Fermi level, which results from the potential perturbation induced by the Si dopants and may contribute the electronic transport through the structure. To further understand the pattern-dependent symmetry in the homogenous Si_xC_{1-x} sheets, we use the superatom model proposed by Shima and Aoki, who have successfully interpreted the electronic structure of superhoneycomb system using group theory.[38] First, the unitcell of the homogenous sheets are considered asa supercell which consists of two superatoms, denoted as α and β (see Figure 4b, c and d). Then the superatoms can be classified into type A_0 when there is a hexagon in the center of each superatom and type A_C when there is an atom. A vector dependence of the classification is identified by defining vectors $\mathbf{R}_\alpha$ and $\mathbf{R}_\beta$ (green arrow in Figure 4) connecting the vertex and the center (red dashed circle) of the superatoms α and β, respectively. According to group theoretical analysis, Shima and Aoki

claimed that the triangular lattices of A_0 and A_C types are semiconducting and semi-metallic, respectively.[38] In a similar way, we find that both the triangular lattices of the semimetallic sheets are composed of two A_C type superatoms, while that of a semiconductive sheet can be considered as consisting of A_0 and A_C type superatoms (in Figure S8). An exception is the (1,0) structure, but its α superatom contains one more Si atom than the β superatom. In this respect, the asymmetry between the two super-atoms is still in place, resulting in the direct band gap. Interestingly, the direct band gap of (1,0) structure is formed at the Γ point, in contrast to those in other semiconductive homogenous sheets that arise at the K point.

CONCLUSIONS:

In summary, we have performed a comprehensive structural search on the 2D Si_xC_{1-x} sheet with $0<x<1$ by using cluster expansion method in conjunction with density functional calculations. All the revealed ground state structures of 2D Si_xC_{1-x} are proved to possess high thermodynamic stability and show strong dependence on x. Generally, we obtained two types of 2D Si_xC_{1-x} structures, a homogenous phase with spatially well dispersed dopants and an in-plane hybrid phase consisting of SiC and graphene (or silicene for $x>0.5$) domains. All the in-plane hybrid structures are semiconductors with a band gap widely tunable with varying x, increasing from 0 eV at $x=0$ or 1 to 2.87 eV at $x=0.5$. The mechanism for the band gap opening can be ascribed to the quantum confinement effect imposed by the SiC domains. In contrast, the homogenous structures can be semiconductive or remain metallic depending on a superlattice vector connecting two adjacent doping sites, complying with a rule similar to the gap-chirality relationship in carbon nanotubes. Our findings feature the Si_xC_{1-x}sheets as a new type of 2D materials with a rich variety of electronic properties for versatile applications, and may open a wealth of opportunities for future development of nanoscale devices that can be integrated seamlessly with existing silicon electronics.

METHODS:

To search the ground state structures at different silicon concentrations, we considered Si_xC_{1-x} as an alloy system and use the state-of-the-art CE method[39] established in the alloy theory, in which the alloy Hamiltonian is mapped onto a generalized Ising Hamiltonian. In the CE formalism, any function of a given configuration $\sigma = \{\sigma_1, \sigma_2, \ldots, \sigma_N\}$ of σ_i is fitted through a multivariate expansion in site occupancy variables (spins) σ_i. Zero-index orthonormal polynomials have the value of 1, and therefore are not included into the sum. For a two-component alloy, the cluster expansion of the mixing energy (per site) can be written as:[40]

$$E(\sigma) = \sum_{\alpha} m_{\alpha} J_{\alpha} \langle \prod_{i \in \alpha} \sigma_i \rangle$$

Here, lattice symmetry has been taken into account by forming symmetry-adapted expansion coefficients for equivalent clusters. Like in the general case, α in this equation enumerates all lattice-symmetry inequivalent subsets (clusters) of a full set of lattice sites, m_α is the number of clusters that are equivalent to α by the lattice symmetry (divided by the total number of lattice sites*N*), and coefficients J_α are the effective cluster interactions (ECI). Angle brackets designate the arithmetic average over all sets of points i={q, q', ..., q''} that are equivalent to the subset represented by α through lattice symmetry. Averaging over the symmetry-equivalent clusters is possible due to the independence of the effective cluster interactions J_α on the spin configurations. This averaging reduces the numbers of independent ECI coefficients. The discrete site occupation variables σ_i are assigned values of +1 and -1in a binary system. The cluster expansions equation converges rapidly with cluster size, yielding an exact result in the untruncated form. In this work, the CE fitting of the mixing energy and the search for the thermodynamic ground state are carried out with the Alloy-Theoretic Automated Toolkit (ATAT) code.[40] The formation energies of alloy structures generated by ATAT and used in the fitting procedure are computed at the density-functional theory (DFT) level. To minimize the effect of lattice mismatch, we divided our CE calculations into two parts: CE-1, from graphene to $Si_{0.5}C_{0.5}$, and CE-2, from $Si_{0.5}C_{0.5}$ to silicene as shown in Figure 1e. Total energies and band structures of the as-produced ground state structures are calculated using Perdew-Burke-Ernzerhof parametrization (PBE) [41] of generalized gradient approximation (GGA) and projector-augmented wave (PAW) potentials,[42-43] as implemented in Vienna Ab Initio Simulation Package (VASP).[44] The plane-wave cutoff is set to 520 eV and the convergence tolerance was set as 10^{-4} eV in electronic steps and 0.05 eV/Å in force. About 12 Å vacuum space is employed to avoid spurious interaction between periodic layers. The Monkhorst-Pack grid *k*-points are employed over the Brillouin zone for all the structures, and k-point densities for different-sized supercells are approximately the same. 21 *k*-points with line mode between the two high symmetry *k*-points are used to further investigate the electronic structures on the basis of the equilibrium structures. To evaluate the relative stability, we collect structures with lowest energies at each concentration and calculate the cohesive energy (E_{coh}) and molar formation energy (δF) for a Si_xC_{1-x} alloy, which are defined as:[45]

$$E_{\mathrm{coh}}(\mathrm{x}) = \frac{E_{\mathrm{total}}}{\mathrm{n}} - xE_{\mathrm{Si}} - (1-x)E_{\mathrm{C}}$$

$$\delta F(\mathrm{x}) = \frac{E_{\mathrm{total}}}{\mathrm{n}} - x\mu_{\mathrm{Si}} - (1-x)\mu_{\mathrm{C}}$$

where the E_{total} and n are the total energy and total number of atoms of the system, E_{Si} and E_C represent chemical potentials of single carbon and silicon atoms, and μ_{Si} and μ_C represent chemical potentials of carbon and silicon in graphene and silicene, respectively. Molecular dynamics (MD) simulations, as implemented in the VASP code, are performed to verify the thermal stability of the Si_xC_{1-x}monolayers with enlarged supercells at 2500 K in a NVT ensemble, which lasted for 10ps with a time step of 1fs.

Supporting Information Available: The Supporting Information is available free of charge *via* the Internet at http://pubs.acs.org.

Acknowledgments: This work was supported by the US Army Research Office MURI grant W911NF-11-1-0362 and by the Office of Naval Research grant N00014-15-1-2372. Computations were performed on the DAVinCI and Sugar clusters sponsored by the NSF grant OCI-0959097 to the Ken Kennedy Institute at Rice.

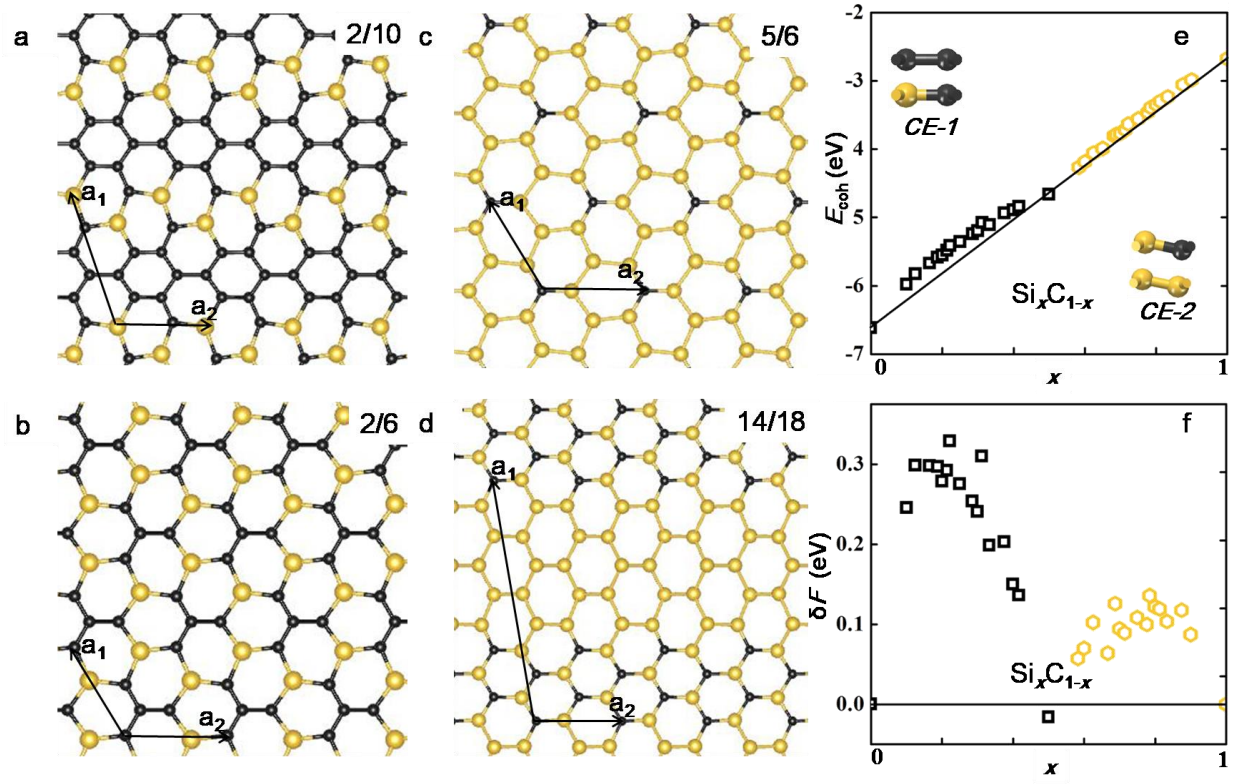

Figure 1. (a)-(d) Atomic structures of four typical Si_xC_{1-x}sheets found by the CE method. The label-fraction represents the ratio of Si and total atoms in a unit cell. (a) and (d) are hybrid structures, (b) and (c) are homogenous structures with well dispersed dopants. (e) and (f) are cohesive energy (E_{coh}) and Molar formation energy (δF) for the ground state Si_xC_{1-x} sheet as the function of x, respectively. Straight line connects E_{coh} and δF of graphene and silicene, respectively. Insets of (e): The top and side views of the primitive cell adopted in CE-1 and CE-2 calculations, respectively. The gray and yellow ball represent the carbon and silicon atoms, and the gray squares and yellow hexagons represent the predicted structures from the CE-1 and CE-2 calculations, respectively.

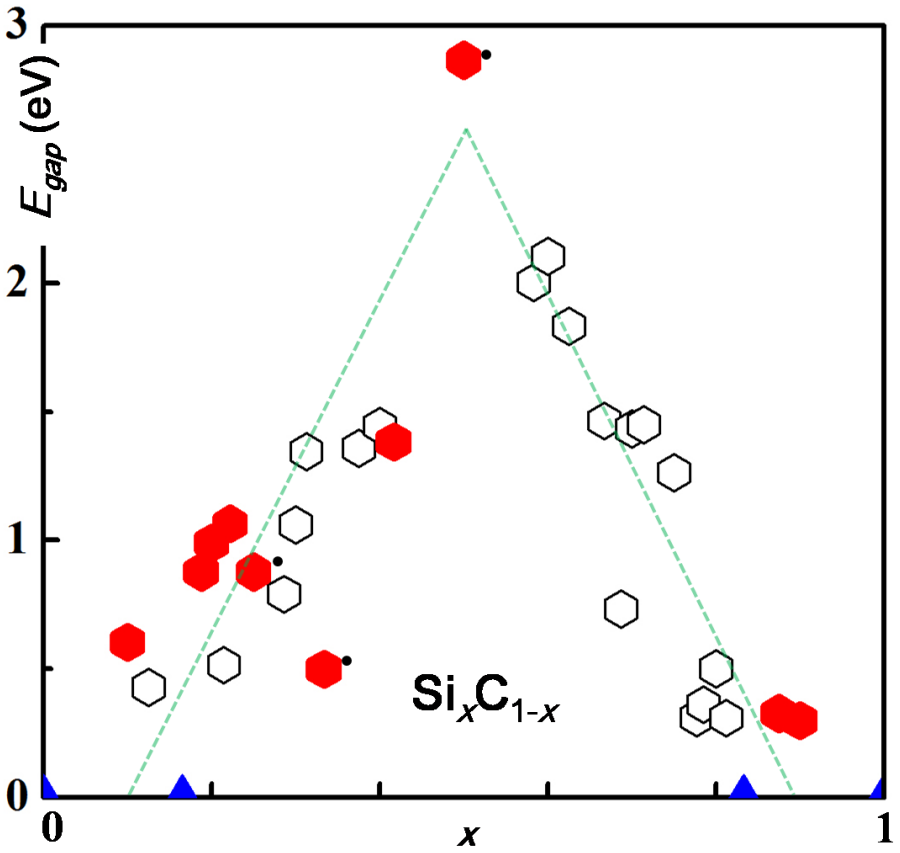

Figure 2. Calculated band gaps of the ground state Si_xC_{1-x} sheets as the function of *x*. Blue solid triangles, black hollow hexagons and red solid hexagons designate semi-metallic, indirect and direct band gap structures, respectively. The structures with black points are reported in previous works,[16, 23, 25] and our results agree with these work.

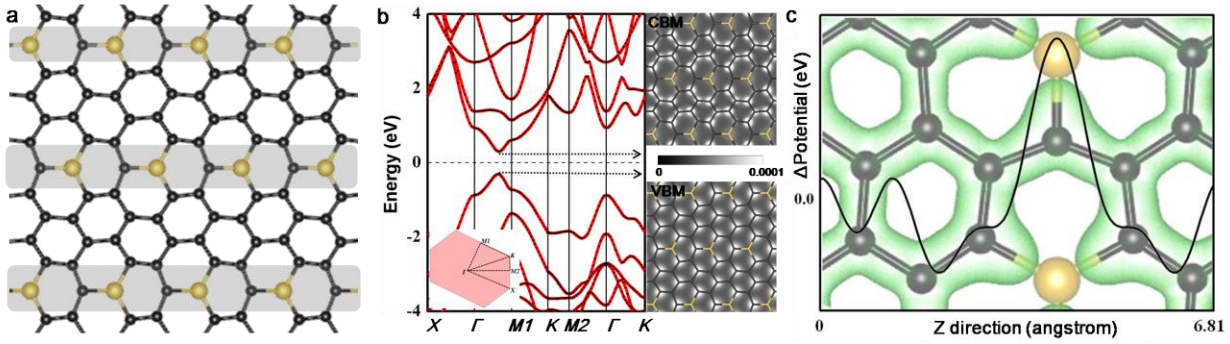

Figure 3. (a) Atomic structure of the $Si_{0.1}C_{0.9}$ sheet. Shaded regions highlight the SiC domains which separate graphene into parallel-aligned nanoribbon. (b) PBE-based band structure and partial charge density corresponding to the VBM and CBM of the $Si_{0.1}C_{0.9}$ sheet. (c) Plane-averaged electrostatic potential along Z direction of the $Si_{0.1}C_{0.9}$ sheet. The background is the charge density together with atomic positions, using the same scale as marked by the horizontal axis.

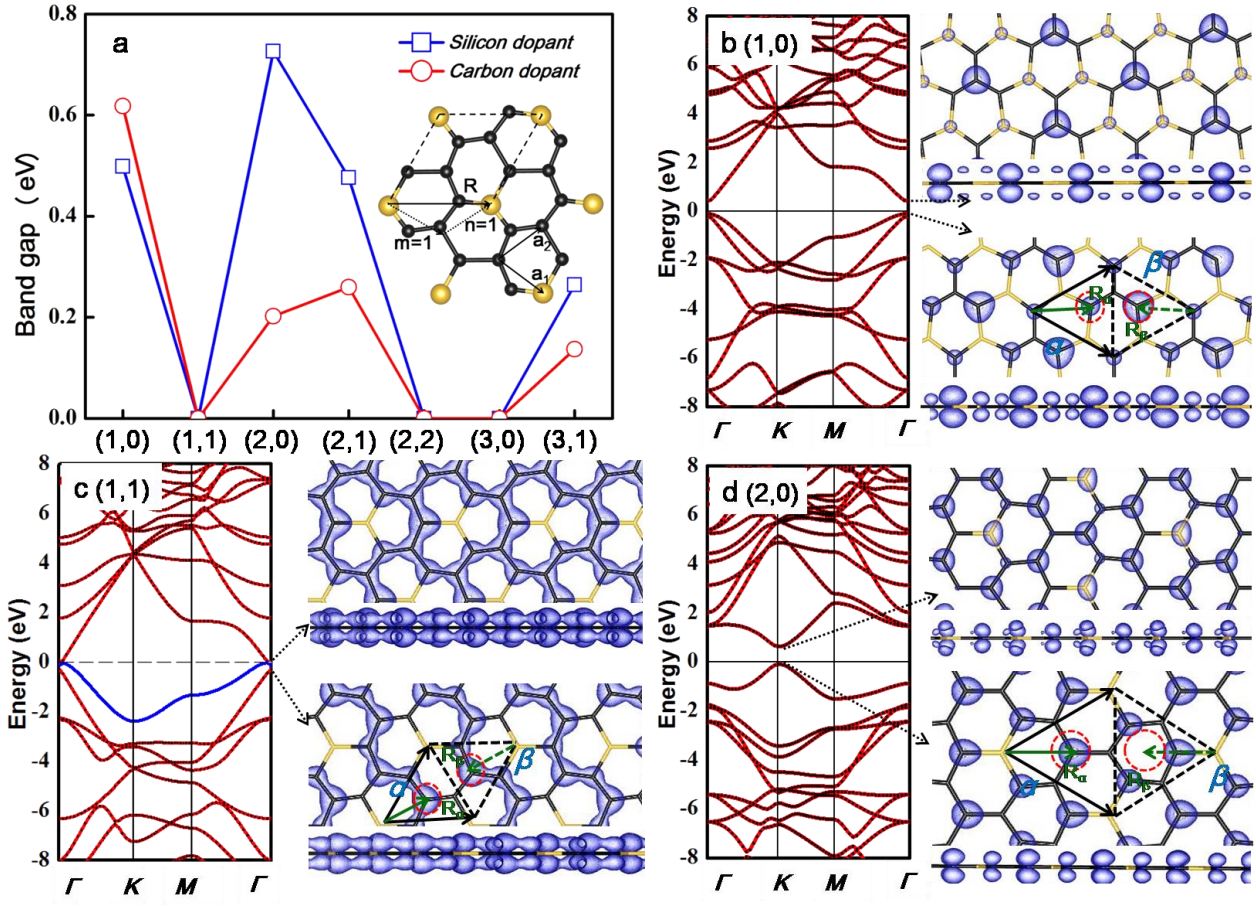

Figure 4. (a) Band gaps of representative homogenous Si_xC_{1-x}structures as a function of superlattice vector ranging from (1,0) to (3,1). Inset is the (1,1) homogenous structure characterized by the superlattice vector $\mathbf{R}=1\mathbf{a}_1+ 1\mathbf{a}_2$.The blue and red lines represent the Si or C doped graphene or silicene, respectively. (b)-(d) Band structures of the (1,0), (1,1) and (2,0) structures and the partial charge densities of the states near the Fermi level. The superatom models are illustrated in each plot of the VBM charge density.

REFERENCES:

1. Novoselov, K. S.; Geim, A. K.; Morozov, S. V.; Jiang, D.; Katsnelson, M. I.; Grigorieva, I. V.; Dubonos, S. V.; Firsov, A. A., Two-Dimensional Gas of Massless Dirac Fermions in Graphene. *Nature* **2005,** *438*, 197-200.
2. Berger, C.; Song, Z. M.; Li, X. B.; Wu, X. S.; Brown, N.; Naud, C.; Mayou, D.; Li, T. B.; Hass, J.; Marchenkov, A. N., *et al.*, Electronic Confinement and Coherence in Patterned Epitaxial Graphene. *Science.* **2006,** *312*, 1191-1196.
3. Zhang, Y. B.; Tan, Y. W.; Stormer, H. L.; Kim, P., Experimental Observation of the Quantum Hall Effect and Berry's Phase in Graphene. *Nature* **2005,** *438*, 201-204.
4. Takeda, K.; Shiraishi, K., Theoretical Possibility of Stage Corrugation in Si and Ge Analogs of Graphite. *Phys. Rev. B.* **1994,** *50*, 14916-14922.
5. Fagan, S. B.; Baierle, R. J.; Mota, R.; da Silva, A. J. R.; Fazzio, A., Ab Initio Calculations for a Hypothetical Material: Silicon Nanotubes. *Phys. Rev. B.* **2000,** *61*, 9994-9996.
6. Guzman-Verri, G. G.; Voon, L. C. L. Y., Electronic Structure of Silicon-Based Nanostructures. *Phys. Rev. B.* **2007,** *76*, 075131.
7. Cahangirov, S.; Topsakal, M.; Akturk, E.; Sahin, H.; Ciraci, S., Two- and One-Dimensional Honeycomb Structures of Silicon and Germanium. *Phys. Rev. Lett.* **2009,** *102*, 236804.
8. Lalmi, B.; Oughaddou, H.; Enriquez, H.; Kara, A.; Vizzini, S.; Ealet, B.; Aufray, B., Epitaxial Growth of a Silicene Sheet. *Appl. Phys. Lett.* **2010,** *97*, 223109.
9. Vogt, P.; De Padova, P.; Quaresima, C.; Avila, J.; Frantzeskakis, E.; Asensio, M. C.; Resta, A.; Ealet, B.; Le Lay, G., Silicene: Compelling Experimental Evidence for Graphenelike Two-Dimensional Silicon. *Phys. Rev. Lett.* **2012,** *108*, 155501.
10. Feng, B. J.; Ding, Z. J.; Meng, S.; Yao, Y. G.; He, X. Y.; Cheng, P.; Chen, L.; Wu, K. H., Evidence of Silicene in Honeycomb Structures of Silicon on Ag(111). *Nano. Lett.* **2012,** *12*, 3507-3511.
11. Chen, L.; Liu, C. C.; Feng, B. J.; He, X. Y.; Cheng, P.; Ding, Z. J.; Meng, S.; Yao, Y. G.; Wu, K. H., Evidence for Dirac Fermions in a Honeycomb Lattice Based on Silicon. *Phys. Rev. Lett.* **2012,** *109*, 056804.
12. Meng, L.; Wang, Y. L.; Zhang, L. Z.; Du, S. X.; Wu, R. T.; Li, L. F.; Zhang, Y.; Li, G.; Zhou, H. T.; Hofer, W. A., *et al.*, Buckled Silicene Formation on Ir(111). *Nano. Lett.* **2013,** *13*, 685-690.
13. Fleurence, A.; Friedlein, R.; Ozaki, T.; Kawai, H.; Wang, Y.; Yamada-Takamura, Y., Experimental Evidence for Epitaxial Silicene on Diboride Thin Films. *Phys. Rev. Lett.* **2012,** *108*, 245501.
14. Yang, L.; Park, C. H.; Son, Y. W.; Cohen, M. L.; Louie, S. G., Quasiparticle Energies and Band Gaps in Graphene Nanoribbons. *Phys. Rev. Lett.* **2007,** *99*, 186801.
15. Ni, Z. Y.; Liu, Q. H.; Tang, K. C.; Zheng, J. X.; Zhou, J.; Qin, R.; Gao, Z. X.; Yu, D. P.; Lu, J., Tunable Bandgap in Silicene and Germanene. *Nano. Lett.* **2012,** *12*, 113-118.
16. Sahin, H.; Cahangirov, S.; Topsakal, M.; Bekaroglu, E.; Akturk, E.; Senger, R. T.; Ciraci, S., Monolayer Honeycomb Structures of Group-Iv Elements and Iii-V Binary Compounds: First-Principles Calculations. *Phys. Rev. B.* **2009,** *80*, 155453.
17. Coleman, J. N.; Lotya, M.; O'Neill, A.; Bergin, S. D.; King, P. J.; Khan, U.; Young, K.; Gaucher, A.; De, S.; Smith, R. J., *et al.*, Two-Dimensional Nanosheets Produced by Liquid Exfoliation of Layered Materials. *Science* **2011,** *331*, 568-571.
18. Zhang, Z. H.; Guo, W. L., Energy-Gap Modulation of Bn Ribbons by Transverse Electric Fields: First-Principles Calculations. *Phys. Rev. B.* **2008,** *77*, 075403.
19. Lin, S. S., Light-Emitting Two-Dimensional Ultrathin Silicon Carbide. *J. Phys. Chem. C.* **2012,** *116*, 3951-3955.
20. Li, H.; Cao, C. B.; Hao, H. W.; Qiu, H. L.; Xu, Y. J.; Zhu, H. S., Self-Assembled One-Dimensional Carbon Nitride Architectures. *Diam. Relat. Mater.* **2006,** *15*, 1593-1600.
21. Chen, S. J.; Liu, Y. C.; Shao, C. L.; Mu, R.; Lu, Y. M.; Zhang, J. Y.; Shen, D. Z.; Fan, X. W., Structural and Optical Properties of Uniform Zno Nanosheets. *Adv. Mater.* **2005,** *17*, 586-590.

22. Zeng, Z. Y.; Yin, Z. Y.; Huang, X.; Li, H.; He, Q. Y.; Lu, G.; Boey, F.; Zhang, H., Single-Layer Semiconducting Nanosheets: High-Yield Preparation and Device Fabrication. *Angew. Chem. Int. Edit.* **2011,** *50*, 11093-11097.
23. Zhou, L. J.; Zhang, Y. F.; Wu, L. M., SiC_2 Siligraphene and Nanotubes: Novel Donor Materials in Excitonic Solar Cells. *Nano. Lett.* **2013,** *13*, 5431-5436.
24. Li, Y. F.; Li, F. Y.; Zhou, Z.; Chen, Z. F., SiC_2 Silagraphene and Its One-Dimensional Derivatives: Where Planar Tetracoordinate Silicon Happens. *J. Am. Chem. Soc.* **2011,** *133*, 900-908.
25. Ding, Y.; Wang, Y. L., Geometric and Electronic Structures of Two-Dimensional SiC_3 Compound. *J. Phys. Chem. C.* **2014,** *118*, 4509-4515.
26. Gao, G. Y.; Ashcroft, N. W.; Hoffmann, R., The Unusual and the Expected in the Si/C Phase Diagram. *J. Am. Chem. Soc.* **2013,** *135*, 11651-11656.
27. Shi, Z. M.; Kutana, A.; Yakobson, B. I., How Much N-Doping Can Graphene Sustain? *J. Phys. Chem. Lett.* **2015,** *6*, 106-112.
28. Kutana, A.; Penev, E. S.; Yakobson, B. I., Engineering Electronic Properties of Layered Transition-Metal Dichalcogenide Compounds through Alloying. *Nanoscale* **2014,** *6*, 5820-5825.
29. Huang, B.; Xiang, H.; Wei, S.-H., Chemical Functionalization of Silicene: Spontaneous Structural Transition and Exotic Electronic Properties. *Phys. Rev. Lett.* **2013,** *111*, 145502.
30. Huang, B.; Xiang, H.; Xu, Q.; Wei, S.-H., Overcoming the Phase Inhomogeneity in Chemically Functionalized Graphene: The Case of Graphene Oxides. *Phys. Rev. Lett.* **2013,** *110*, 085501.
31. Sun, L.; Li, Y. F.; Li, Z. Y.; Li, Q. X.; Zhou, Z.; Chen, Z. F.; Yang, J. L.; Hou, J. G., Electronic Structures of Sic Nanoribbons. *J. Chem. Phys.* **2008,** *129*, 174114.
32. Li, P. F.; Zhou, R. L.; Zeng, X. C., The Search for the Most Stable Structures of Silicon-Carbon Monolayer Compounds. *Nanoscale* **2014,** *6*, 11685-11691.
33. Wang, Y. C.; Miao, M. S.; Lv, J.; Zhu, L.; Yin, K. T.; Liu, H. Y.; Ma, Y. M., An Effective Structure Prediction Method for Layered Materials Based on 2D Particle Swarm Optimization Algorithm. *J. Chem. Phys.* **2012,** *137*, 224108.
34. Son, Y. W.; Cohen, M. L.; Louie, S. G., Energy Gaps in Graphene Nanoribbons. *Phys. Rev. Lett.* **2006,** *97*, 216803.
35. Seol, G.; Guo, J., Bandgap Opening in Boron Nitride Confined Armchair Graphene Nanoribbon. *Appl. Phys. Lett.* **2011,** *98*, 143107.
36. Saito, R.; Fujita, M.; Dresselhaus, G.; Dresselhaus, M. S., Electronic-Structure of Graphene Tubules Based on C-60. *Phys. Rev. B.* **1992,** *46*, 1804-1811.
37. Liu, X. F.; Zhang, Z. H.; Guo, W. L., Universal Rule on Chirality-Dependent Bandgaps in Graphene Antidot Lattices. *Small.* **2013,** *9*, 1405-1410.
38. Shima, N.; Aoki, H., Electronic-Structure of Superhoneycomb Systems - a Peculiar Realization of Semimetal Semiconductor Classes and Ferromagnetism. *Phys. Rev. Lett.* **1993,** *71*, 4389-4392.
39. Sanchez, J. M.; Ducastelle, F.; Gratias, D., Generalized Cluster Description of Multicomponent Systems. *Physica A* **1984,** *128*, 334-350.
40. van de Walle, A.; Asta, M.; Ceder, G., The Alloy Theoretic Automated Toolkit: A User Guide. *Calphad* **2002,** *26*, 539-553.
41. Perdew, J. P.; Burke, K.; Ernzerhof, M., Comment on "Generalized Gradient Approximation Made Simple" - Reply. *Phys. Rev. Lett.* **1998,** *80*, 891-891.
42. Blochl, P. E., Projector Augmented-Wave Method. *Phys. Rev. B.* **1994,** *50*, 17953-17979.
43. Kresse, G.; Joubert, D., From Ultrasoft Pseudopotentials to the Projector Augmented-Wave Method. *Phys. Rev. B.* **1999,** *59*, 1758-1775.
44. Kresse, G.; Furthmuller, J., Efficient Iterative Schemes for Ab Initio Total-Energy Calculations Using a Plane-Wave Basis Set. *Phys. Rev. B.* **1996,** *54*, 11169-11186.
45. Dumitrica, T.; Hua, M.; Yakobson, B. I., Endohedral Silicon Nanotubes as Thinnest Silicide Wires. *Phys. Rev. B.* **2004,** *70*, 241303.

TABLE OF CONTENTS: